Intermetallics 175 (2024) 108500

Contents lists available at ScienceDirect

Intermetallics

journal homepage: www.elsevier.com/locate/intermet

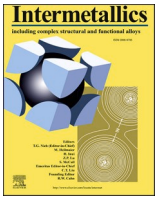

Short-term tensile creep behavior of CoCrNi-based multi-principal element alloys

Kaiju Lu *, Jarir Aktaa

Institute for Applied Materials, Karlsruhe Institute of Technology (KIT), Hermann-von-Helmholtz-Platz 1, 76344, Eggenstein-Leopoldshafen, Germany

ARTICLE INFO

Keywords:
Multi-principal element alloy (MPEA)
Creep
Grain size
Elevated-temperature
Mechanism

ABSTRACT

We report the short-term tensile creep behavior of CoCrFeMnNi and CoCrNi model MPEAs at 550 °C. Dislocation glide and dislocation-dislocation/lattice interactions are proposed to be dominated deformation mechanisms for CoCrFeMnNi and CoCrNi, respectively. Besides, compared to CoCrFeMnNi, CoCrNi exhibits lower creep rate and longer rupture time at same testing conditions. This is attributed to CoCrNi's lower stacking fault energy and higher lattice friction. Additionally, the effect of grain size on the short-term creep behavior of CoCrFeMnNi was revealed.

1. Introduction

In the past two decades, multi-principal element alloys (MPEAs) consisting of three to five principal elements, have been gaining increasing interest. The most investigated face-centered cubic (FCC) single-phase MPEAs are the CoCrNi-based alloys (such as CoCrNi and CoCrFeMnNi), which are regarded as model MPEAs and promising engineering materials due to their excellent mechanical properties, fatigue and fracture toughness [1–5]. At elevated temperatures, in spite of their excellent oxidation and corrosion resistance [6], the strength of CoCrNi-based FCC MPEAs is often inadequate, limiting their wide applications [7]. However, based on the CoCrNi matrix, the advancement of oxide dispersion-strengthened (ODS) MPEAs and high-entropy superalloys (HESAs) has shown promising elevated-temperature strength, which is comparable or even superior to Ni-based superalloys [7–9]. Therefore, it is essential to understand the deformation behaviors (such as tension/compression [10,11], fatigue [12–14] and creep) of the CoCrNi-based matrix alloys at elevated temperatures, which can serve as prerequisite for modeling and developing more complex CoCrNi-based ODS MPEAs or HESAs [7,15].

Recently, much attention has been placed on the elevated-temperature creep properties of FCC MPEAs [15–18]. For instance, Kang et al. [16] investigated the long-term creep performance of CoCrFeMnNi at temperatures of 535–650 °C and under stresses of 20–100 MPa. They found the creep deformation mechanisms' transition from dislocation climb to dislocation glide, accompanied by a change in stress exponent from low stress regime to high stress regime [16]. Rozman et al. [19,20] have reported the long-term creep behaviors of CoCrFeMnNi and CoCrFeNi alloys at temperatures of 600–650 °C and under stresses of 120–189 MPa. They found that the stress exponent of CoCrFeMnNi is ≈ 6.3, and that of CoCrFeNi is within the range of 6.3–7.5. These values indicate that dislocation glide combined with cross slip and climb as primary deformation mechanisms [19,20]. Xie et al. [18,21] studied long-term creep behaviors of CoCrNi, CoCrFeNi and CoCrFeMnNi alloys at temperatures of 700–800 °C and under stresses of 30–140 MPa. Their results displayed that CoCrNi and CoCrFeNi show lower stress exponent ≈5.4–5.5 as compared to CoCrFeMnNi (≈6.0), suggesting dislocation climb as dominant deformation mechanisms [21]. Zhang et al. [17] reported a much lower stress exponent of ≈3.7 for CoCrFeMnNi by performing creep tests under stresses of 20–200 MPa and at temperatures of 750–900 °C.

It should be mentioned that the above studies mainly focused on the long-term creep behaviors (e.g., lifetime >200 h) of FCC MPEAs, with few studies covering their short-term creep behaviors (e.g., lifetime ≤200 h) at intermediate temperatures. Besides, the question of how the grain size of FCC MPEAs affects their creep behaviors also remains unexplored.

Consequently, this work aims to fill these gaps and provide short-term creep deformation behaviors of CoCrFeMnNi (with two distinct average gran sizes) and CoCrNi model MPEAs at an intermediate temperature of 550 °C (which lies within the proposed operating temperature range of advanced power plants and nuclear reactors [22–24]).

* Corresponding author.
E-mail addresses: kaiju.lu@hotmail.com, kaiju.lu@kit.edu (K. Lu).

https://doi.org/10.1016/j.intermet.2024.108500
Received 31 May 2024; Received in revised form 2 September 2024; Accepted 15 September 2024
Available online 22 September 2024

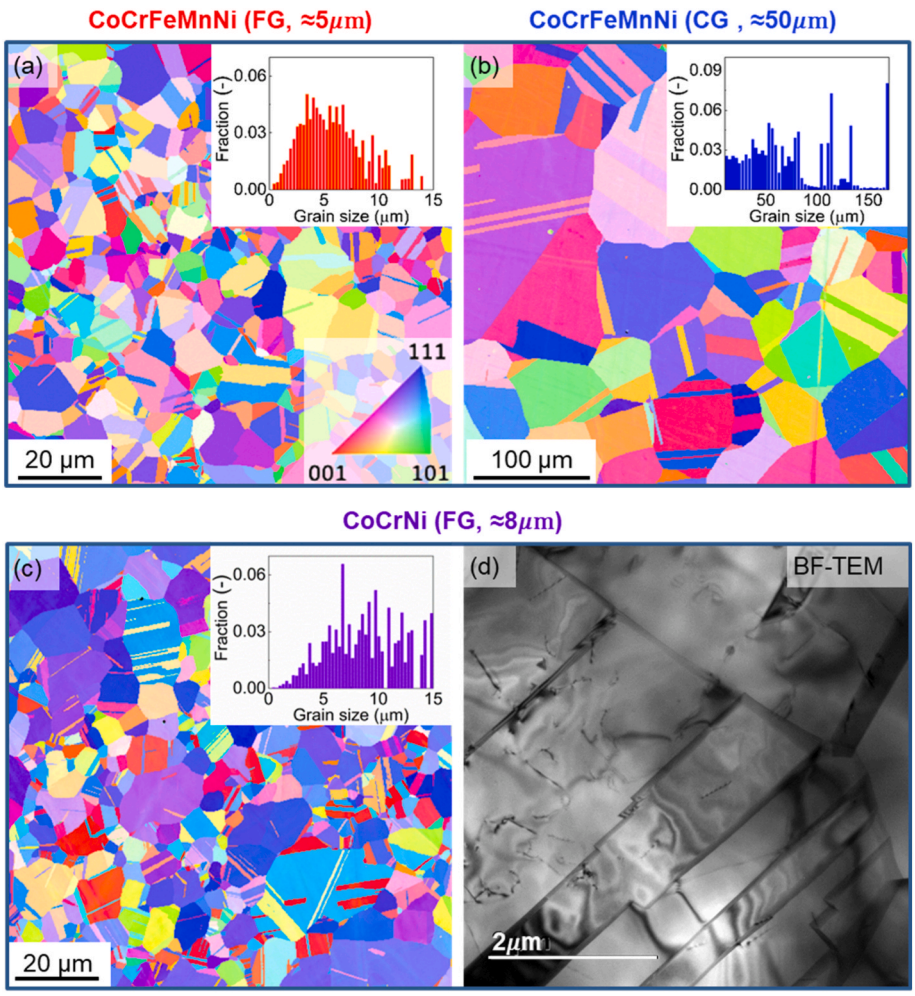

Fig. 1. (a–b) Microstructures of the CoCrFeMnNi alloy annealed at 800 °C (a) and 1000 °C (b), as well as of the CoCrNi alloy annealed at 825 °C (c–d). Figures (a–c) are representative IPF maps along the swaging direction and have been reported in Refs. [25,28]. The insets in (a–c) provide the grain size distributions of each state (where the twin boundaries were included during calculating grain sizes). Figure (d) is an example BF-TEM micrograph illustrating low initial dislocation density after annealing at the three conditions.

2. Experimental details

The investigated CoCrFeMnNi and CoCrNi alloys were synthesized from pure metals (with at least 99.9 wt% purity) by arc melting and vacuum induction, respectively, followed by casting. The as-cast CoCrFeMnNi and CoCrNi ingots were homogenized at 1200 °C for 72 h and 48 h, respectively, followed by water-quenching. Subsequently the alloys were rotary swaged. More details about the processing can be found in Ref. [25].

For performing creep tests, flat dog-bone shaped micro-specimens (with a gauge length of ≈1 mm, a gauge width of ≈0.3 mm and a gauge thickness of ≈0.12 mm) were machined out from the rotary-swaged rods by micro-electric discharge machining [26]. Then the CoCrFeMnNi alloy was annealed for 1 h at 800 °C and 1000 °C, respectively, to obtain two different grain sizes (with at least one-order magnitude difference). The CoCrNi alloy was annealed for 1 h at 825 °C to receive a similar average grain size as one of the CoCrFeMnNi alloy. The initial microstructures of these alloys were characterized using electron backscatter diffraction (EBSD) and transmission electron microscopy (TEM). EBSD investigations were performed using an FEI 200 Dual-Beam SEM/FIB equipped with an HKL EBSD detector with step size of 200 nm at 20 kV. TEM investigations were carried out using a Gatan F20 microscope.

Creep tests were performed in air using an in-house micro-creep testing setup [26]. The tests were carried out at 550 °C with constant applied stresses from 180 MPa to 280 MPa. The stresses were chosen to ensure that the fracture lifetime is within 2 weeks (i.e., at short-term creep stage). After testing, the true strain was calculated by Digital Imaging Correlation using open-source Matlab scripts [27]. To understand creep damage mechanisms, specimens' surface and fracture surface were examined using a Zeiss EVO MA 10 SEM.

3. Results and discussion

The representative inverse pole figure (IPF) maps of CoCrFeMnNi and CoCrNi alloys after annealing at the above-mentioned three conditions (prior to creep testing) are shown in Fig. 1a–c, respectively. It can be seen that the investigated CoCrFeMnNi and CoCrNi alloys have FCC single-phase, a high density of annealing twins and a weak texture (Fig. 1a–c). Besides, the insets in Fig. 1a–b shows that the CoCrFeMnNi alloys annealed at 800 °C and 1000 °C have average grain sizes of ≈5 μm and ≈50 μm, respectively, which are referred to as fine-grained (FG) and coarse-grained (CG) hereafter. In addition, the inset in Fig. 1c displays that the average grain size of the CoCrNi alloy is ≈ 8 μm, similar to the FG CoCrFeMnNi alloy. Furthermore, the CoCrFeMnNi and CoCrNi alloys both possess low initial dislocation densities, indicating fully recrystallized microstructures (*see* a typical TEM micrograph in Fig. 1d). Together, these similarities allow a relatively fair comparison between

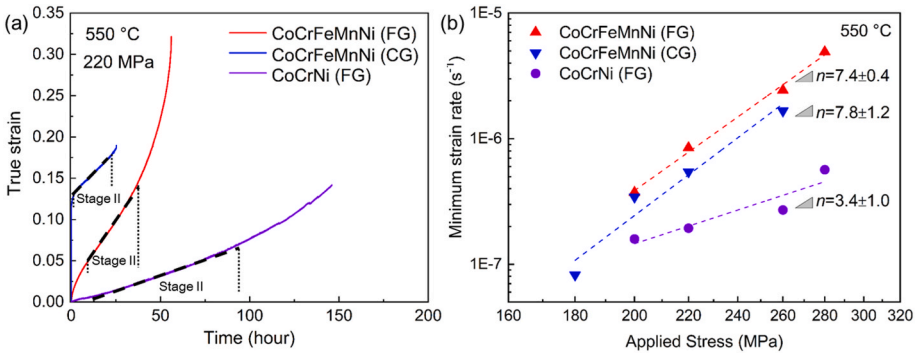

Fig. 2. (a) Typical tensile creep curves tested under applied stress of 220 MPa and 550 °C, (b) double-logarithmic plots of minimum strain rate *versus* applied stress for FG and CG CoCrFeMnNi, as well as FG CoCrNi at 550 °C. The fitted n values using equation (1) are also provided in (b).

Table 1
A comparison of creep experiments for CoCrFeMnNi and CoCrNi MPEAs.

Materials	Average grain size (μm)	Tempe-rature (°C)	Stress range σ (MPa)	Stress exponent n	Mechanisms	Ref.
CoCrFeMnNi	≈50	550	180–280	7.8 ± 1.2	Dislocation glide	This work
	≈5			7.4 ± 0.4		
	≈25	500, 550, 600	140–400	5-6 (low σ); 8.9–14 (high σ)	Dislocation climb; Dynamic recrystallization, precipitation, and dislocation climb	[31]
	≈21.7	535, 650	20–40 50–100	≈6 (low σ); ≈3 (high σ)	Dislocation climb; Dislocation glide	[16]
	≈24	800, 850, 900, 950	40, 60, 80	≈3.7	Dislocation and dislocation/lattice interactions	[17]
	≈18	575–650	103–207	≈6.2	Dislocation creep	[19]
	≈140-150	700	50–110	6.0	Dislocation creep	[21]
CoCrNi	≈8	550	180–280	3.4 ± 1.0	Dislocation and dislocation/lattice interactions	This work
	≈150	700, 750, 800	50–130	5.5	Dislocation climb and lattice diffusion	[18]

the FG CoCrFeMnNi and CoCrNi alloys.

Typical creep curves of the three alloys tested at 550 °C and 220 MPa are shown in Fig. 2a, which shows the true strain as a function of time. The curves of the CoCrFeMnNi and CoCrNi alloys feature classic primary, secondary and tertiary regions. For simplicity, only the secondary stage (II) were marked in Fig. 2a. The classic primary creep stage is linked with the decreased density of mobile dislocation and the formation of dislocation substructures till reaching the steady state, as often observed in pure metals and class *M* alloys [29]. These trends are also valid for the alloys tested at other stress levels from 180 MPa to 280 MPa at 550 °C (not shown here for brevity).

The secondary creep stage takes up the majority of the creep lifetime t_r (Fig. 2a). The minimum creep rate $\dot{\varepsilon}$ at secondary steady-state was plotted against the applied stress as shown in Fig. 2b and fitted by the power law equation [30]:

$$\dot{\varepsilon} = A\sigma^n \exp\left(-\frac{Q_c}{RT}\right) \quad (1)$$

where A is a material constant, n is the stress exponent, Q_c is the activation energy of creep, R is the ideal gas constant, and T is the absolute temperature. The fitted slopes in Fig. 2b represent the stress exponent n values, which were also given in Fig. 2b and Table 1. Despite the deviation from scatter, the minimum strain rate and the applied stress follow the above power-law equation fairly-well.

For comparison, the creep testing results of CoCrFeMnNi and CoCrNi obtained from other studies were also provided in Table 1. Evidently, the n values of the present FG and CG CoCrFeMnNi tested at short-term creep stage and 550 °C are around 7.4–7.8, which is close to the values of CoCrFeMnNi tested at long-term stage and 600–650 °C (i.e., around 6.3–7.5) [19,20]. This suggests that the short-term creep deformation of FG and CG CoCrFeMnNi is carried by dislocation glide

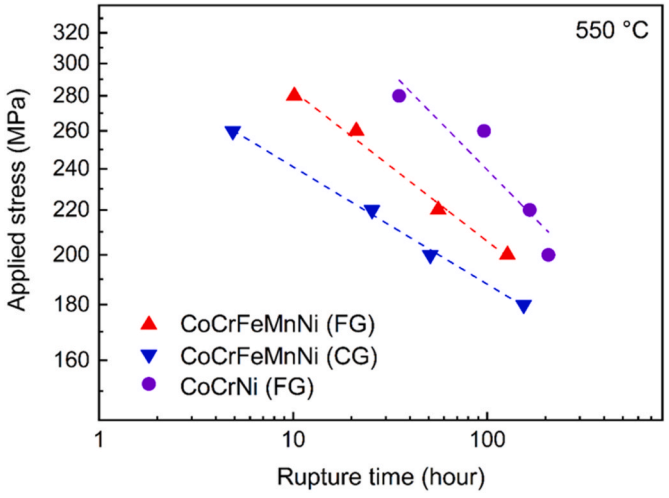

Fig. 3. (a) Applied stress, and (b) minimum strain rate *versus* rupture time of FG and CG CoCrFeMnNi, as well as FG CoCrNi crepted at 550 °C.

[19,20]. On the other hand, the n value of the present CoCrNi tested at short-term creep stage and 550 °C is around 3.4, which is close to the value of CoCrFeMnNi tested at long-term stage and 750–900 °C (i.e., around 3.7). This implies that the short-term creep of CoCrNi is dominated by dislocation-dislocation interactions and dislocation-lattice interactions [17]. To verify the operating creep deformation mechanisms and probe the difference of the two alloys, further dedicated microstructural investigations are warranted and shall be reported in the future.

Table 2
Fitted parameters B and r from the relationship of creep lifetime and applied stress of CoCrFeMnNi and CoCrNi MPEAs.

Materials	Parameter B	Parameter r
FG CoCrFeMnNi	390.75	7.18
CG CoCrFeMnNi	308.06	9.24
FG CoCrNi	640.56	4.80

The applied stress σ *versus* creep rupture time t_r curves of the investigated alloys were plotted in Fig. 3. The creep rupture time t_r and applied stress σ were fitted using the equation of $t_r=(\sigma/B)\hat{}\text{-}r$. Here B and r are materials constant. Their fitted values were given in Table 2.

As evident from Fig. 3, under the same stress levels, the FG CoCrFeMnNi shows longer creep rupture time as compared to the CG CoCrFeMnNi, which can be ascribed to grain boundary strengthening. Furthermore, the CoCrNi exhibits longer rupture time than that of the CoCrFeMnNi alloys, due to the CoCrNi's higher yield strength. Notably, the yield strength of current CG and FG CoCrFeMnNi as well as FG CoCrNi at 550 °C is around 120 MPa, 227 MPa and 312 MPa, respectively (which are estimated from the stress-strain curves in our previous work [14] and Ref. [32]). The higher yield strength of CoCrNi originates from both higher grain boundary strengthening and solid solution strengthening ability, due to its lower stacking fault energy and higher lattice friction than CoCrFeMnNi [14].

Additionally, it is of interest to compare the creep behaviors of the current FCC CoCrNi-based MPEA with those of conventional austenitic steels [33,34] (such as 316 L(N) steels). Since the data of steels tested at the same conditions are not available, the available data of 316 L(N) steels tested at a higher temperature of 650 °C were provided below to give first insights on the comparison. Specifically, it was reported that for Nitrogen alloyed 316 L(N) steels, the creep rupture lifetimes ranged from 100 to 1000 h at temperature of **650 °C** and stress of 200 MPa [34]. These rupture lifetimes are longer than that of the current CoCrNi-based MPEAs (i.e., 40–200 h, *see* Fig. 3) tested at **550 °C** and a same stress of 200 MPa. Therefore, the 316 L N steels are expected to perform better (i.e., having longer lifetime) at the same temperature of 550 °C and 220 MPa than the current MPEAs. The superior creep behavior of 316 L(N) steels than the MPEAs may stem from the beneficial effects of interstitial Nitrogen and Carbon contents, including solid solution strengthening, increase in Young's modulus, decrease in stacking fault energy and matrix precipitation strengthening of carbonitride precipitates [34]. In this context, the incorporation of Nitrogen and Carbon in the MPEAs are anticipated to improve creep resistance of CoCrNi-based MPEAs, which requires further investigations in the future.

Typical SEM micrographs of the specimens' surface and fracture surface for CoCrFeMnNi and CoCrNi alloys are shown in Fig. 4a–c to reveal their creep damage mechanisms. It can be seen that from the specimens' surface, both CoCrFeMnNi and CoCrNi show creep cavities, irrespective of grain size (see Fig. 4a_1, b_1, and c_1). However, their fracture surfaces exhibit different features. Specifically, the FG CoCrFeMnNi and CoCrNi alloys display ductile dimple feature; while the CG CoCrFeMnNi shows non-ductile cleavage feature that suggests an intergranular fracture mechanism and is correlated with the shorter rupture lifetime in the latter alloy.

4. Conclusion

This work revealed the short-term creep deformation behaviors of the fine-grained (FG) and coarse-grained (CG) CoCrFeMnNi, as well as fine-grained (FG) CoCrNi MPEAs under stress of 180–280 MPa at 550 °C. Key findings are summarized as follows:

(1) At the investigated conditions, as suggested by the fitted stress exponent n, the creep mechanisms of FG and CG CoCrFeMnNi alloys (of n value of 7.4–7.8) are dislocation-glide. On the other hand, the creep of CoCrNi alloy (of n value of around 3.4) is characterized by dislocation-dislocation and dislocation-lattice interactions.
(2) At the same stress levels, the CoCrNi alloy exhibits longer creep lifetime and lowest creep rates, due to its higher strength from grain boundary strengthening and solid solution strengthening ability than the CoCrFeMnNi alloy. Besides, the FG CoCrFeMnNi alloy shows longer creep lifetime and lower strain rate owing to its higher grain boundary strengthening than its CG counterpart.
(3) Both the CoCrFeMnNi and CoCrNi alloys show creep cavities after creep testing. The FG CoCrFeMnNi and CoCrNi alloys display ductile fracture. However, the CG CoCrFeMnNi alloy exhibits

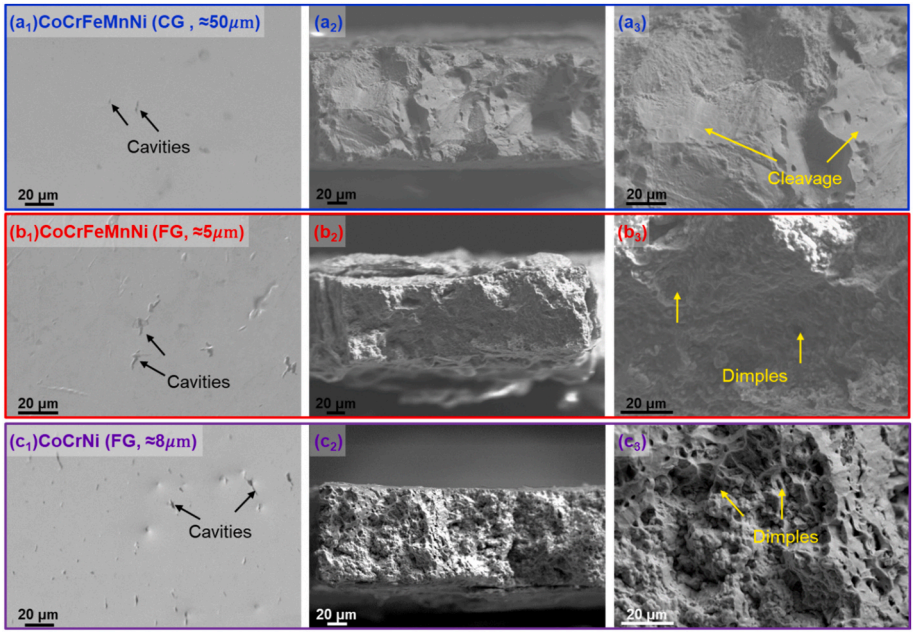

Fig. 4. SEM micrographs of ($a_{1\text{-}3}$) CG and ($b_{1\text{-}3}$) FG CoCrFeMnNi, as well as ($c_{1\text{-}3}$) FG CoCrNi crepted at 550 °C until fracture. (a_1, b_1 and c_1) were acquired from specimens' surface; while the rest (a_2-c_2, a_3-c_3) were obtained from the corresponding fracture surfaces.

non-ductile intergranular fracture, which well explained its lowest creep lifetime.

(4) The CoCrNi and CoCrFeMnNi appear to show inferior creep properties as compared to Nitrogen-alloyed 316L(N) steels, probably due to the beneficial effects from interstitial Nitrogen and Carbon contents (including solid solution strengthening, increase in Young's modulus, decrease in stacking fault energy and matrix precipitation strengthening of carbonitride precipitates) in the latter.

CRediT authorship contribution statement

Kaiju Lu: Writing – original draft, Investigation, Formal analysis, Data curation, Conceptualization. **Jarir Aktaa:** Writing – review & editing, Supervision, Resources, Project administration, Funding acquisition.

Declaration of competing interest

The authors declare that they have no known competing financial interests or personal relationships that could have appeared to influence the work reported in this paper.

Data availability

Data will be made available on request.

Acknowledgments

The authors acknowledge Prof. Dr. M. Heilmaier and Prof. G. Laplanche for providing the investigated materials, as well as Prof. Dr. J. Freudenberger for performing rotary-swaging for the materials.

References

[1] K. Lu, A. Chauhan, D. Litvinov, M. Schneider, G. Laplanche, J. Aktaa, Cooperative deformation mechanisms in a fatigued CoCrNi multi-principal element alloy: a case of low stacking fault energy, J. Mech. Phys. Solid. 180 (2023) 105419.
[2] B. Gludovatz, A. Hohenwarter, K.V. Thurston, H. Bei, Z. Wu, E.P. George, R. O. Ritchie, Exceptional damage-tolerance of a medium-entropy alloy CrCoNi at cryogenic temperatures, Nat. Commun. 7 (2016) 10602.
[3] G. Laplanche, A. Kostka, C. Reinhart, J. Hunfeld, G. Eggeler, E.P. George, Reasons for the superior mechanical properties of medium-entropy CrCoNi compared to high-entropy CrMnFeCoNi, Acta Mater. 128 (2017) 292–303.
[4] D. Hua, Q. Xia, W. Wang, Q. Zhou, S. Li, D. Qian, J. Shi, H. Wang, Atomistic insights into the deformation mechanism of a CoCrNi medium entropy alloy under nanoindentation, Int. J. Plast. 142 (2021) 102997.
[5] D. Liu, Q. Yu, S. Kabra, M. Jiang, P. Forna-Kreutzer, R. Zhang, M. Payne, F. Walsh, B. Gludovatz, M. Asta, A.M. Minor, E.P. George, R.O. Ritchie, Exceptional fracture toughness of CrCoNi-based medium- and high-entropy alloys at 20 kelvin, Science 378 (6623) (2022) 978–983.
[6] C. Stephan-Scherb, W. Schulz, M. Schneider, S. Karafiludis, G. Laplanche, High-temperature oxidation in dry and humid atmospheres of the equiatomic CrMnFeCoNi and CrCoNi high- and medium-entropy alloys, Oxid. Metals 95 (1) (2021) 105–133.
[7] M. Zhang, E.P. George, J.C. Gibeling, Elevated-temperature deformation mechanisms in a CrMnFeCoNi high-entropy alloy, Acta Mater. 218 (2021).
[8] T.M. Smith, C.A. Kantzos, N.A. Zarkevich, B.J. Harder, M. Heczko, P.R. Gradl, A. C. Thompson, M.J. Mills, T.P. Gabb, J.W. Lawson, A 3D printable alloy designed for extreme environments, Nature 617 (2023) 513–518.
[9] Y. Zhang, K. Lu, F. Jiang, Y. Chen, X. Liang, Superior strength-ductility synergy of an oxide-dispersion strengthened CoCrNi-based multi-principal element alloy, Mater. Res. Lett. 12 (11) (2024) 825–833.
[10] M. Kawamura, M. Asakura, N.L. Okamoto, K. Kishida, H. Inui, E.P. George, Plastic deformation of single crystals of the equiatomic Cr−Mn−Fe−Co−Ni high-entropy alloy in tension and compression from 10 K to 1273 K, Acta Mater. 203 (2021) 116454.
[11] L. Li, Z. Chen, S. Kuroiwa, M. Ito, K. Kishida, H. Inui, E.P. George, Tensile and compressive plastic deformation behavior of medium-entropy Cr-Co-Ni single crystals from cryogenic to elevated temperatures, Int. J. Plast. 148 (2021) 103144.
[12] K. Lu, A. Chauhan, D. Litvinov, M. Walter, A.S. Tirunilai, J. Freudenberger, A. Kauffmann, M. Heilmaier, J. Aktaa, High-temperature low cycle fatigue behavior of an equiatomic CoCrFeMnNi high-entropy alloy, Mater. Sci. Eng., A 791 (2020) 139781.
[13] K. Lu, A. Chauhan, D. Litvinov, J. Aktaa, Temperature-dependent cyclic deformation behavior of CoCrFeMnNi high-entropy alloy, Int. J. Fatig. 160 (2022) 106863.
[14] K. Lu, F. Knöpfle, A. Chauhan, D. Litvinov, M. Schneider, G. Laplanche, J. Aktaa, Elevated-temperature cyclic deformation mechanisms of CoCrNi in comparison to CoCrFeMnNi, Scripta Mater. 220 (2022) 114926.
[15] G. Sahragard-Monfared, M. Zhang, T.M. Smith, A.M. Minor, J.C. Gibeling, Superior tensile creep behavior of a novel oxide dispersion strengthened CrCoNi multi-principal element alloy, Acta Mater. (2023) 119032.
[16] Y.B. Kang, S.H. Shim, K.H. Lee, S.I. Hong, Dislocation creep behavior of CoCrFeMnNi high entropy alloy at intermediate temperatures, Mater. Res. Lett. 6 (12) (2018) 689–695.
[17] M. Zhang, E.P. George, J.C. Gibeling, Tensile creep properties of a CrMnFeCoNi high-entropy alloy, Scripta Mater. 194 (2021).
[18] D. Xie, R. Feng, P.K. Liaw, H. Bei, Y. Gao, Tensile creep behavior of an equiatomic CoCrNi medium entropy alloy, Intermetallics 121 (2020).
[19] K.A. Rozman, M. Detrois, T. Liu, M.C. Gao, P.D. Jablonski, J.A. Hawk, Long-term creep behavior of a CoCrFeNiMn high-entropy alloy, J. Mater. Eng. Perform. 29 (9) (2020) 5822–5839.
[20] K.A. Rozman, M. Detrois, M.C. Gao, P.D. Jablonski, J.A. Hawk, Long-term creep behavior of a CoCrFeNi medium-entropy alloy, J. Mater. Eng. Perform. 31 (2022) 9220–9235.
[21] D. Xie, R. Feng, P.K. Liaw, H. Bei, Y. Gao, Long-term tensile creep behavior of a family of FCC-structured multi-component equiatomic solid solution alloys, Scripta Mater. 212 (2022).
[22] A. Chauhan, D. Litvinov, J. Aktaa, Deformation and damage mechanisms of a bimodal 12Cr-ODS steel under high-temperature cyclic loading, Int. J. Fatig. 93 (2016) 1–17.
[23] B. Li, Y. Zheng, J. Zhao, S. Shi, Z. Zhang, X. Chen, Cyclic deformation behavior and dynamic strain aging of 316LN stainless steel under low cycle fatigue loadings at 550°C, Mater. Sci. Eng., A 818 (2021).
[24] A. Chauhan, J. Hoffmann, D. Litvinov, J. Aktaa, High-temperature low-cycle fatigue behavior of a 9Cr-ODS steel: Part 1 - pure fatigue, microstructure evolution and damage characteristics, Mater. Sci. Eng., A 707 (2017) 207–220.
[25] K. Lu, A. Chauhan, M. Walter, A.S. Tirunilai, M. Schneider, G. Laplanche, J. Freudenberger, A. Kauffmann, M. Heilmaier, J. Aktaa, Superior low-cycle fatigue properties of CoCrNi compared to CoCrFeMnNi, Scripta Mater. 194 (2021) 113667.
[26] K. Lu, A. Chauhan, D. Litvinov, A.S. Tirunilai, J. Freudenberger, A. Kauffmann, M. Heilmaier, J. Aktaa, Micro-mechanical deformation behavior of CoCrFeMnNi high-entropy alloy, J. Mater. Sci. Technol. 100 (2022) 237–245.
[27] C. Eberl, R. Thompson, D. Gianola, W.J. Sharpe, K.J. Hemker, Digital image correlation and tracking, MatLabCentral, Mathworks file exchange server, MatLab Central, Mathworks file exchange server (2006).
[28] K. Lu, A. Chauhan, A.S. Tirunilai, J. Freudenberger, A. Kauffmann, M. Heilmaier, J. Aktaa, Deformation mechanisms of CoCrFeMnNi high-entropy alloy under low-cycle-fatigue loading, Acta Mater. 215 (2021) 117089.
[29] P. Yavari, F.A. Mohamed, T.G. Langdon, Creep and substructure formation in an Al-5% Mg solid solution alloy, Acta Metall. 29 (8) (1981) 1495–1507.
[30] A.K. Mukherjee, J.E. Bird, J.E. Dorn, Experimental Correlations for High-Temperature Creep, Report, 1968. UCRL-18526.
[31] C. Cao, J. Fu, T. Tong, Y. Hao, P. Gu, H. Hao, L. Peng, Intermediate-temperature creep deformation and microstructural evolution of an equiatomic FCC-structured CoCrFeNiMn high-entropy alloy, Entropy 20 (12) (2018).
[32] F. Otto, A. Dlouhý, C. Somsen, H. Bei, G. Eggeler, E.P. George, The influences of temperature and microstructure on the tensile properties of a CoCrFeMnNi high-entropy alloy, Acta Mater. 61 (15) (2013) 5743–5755.
[33] T. Sritharan, H. Jones, The creep of type 304 stainless steel at low stresses, Acta Metall. 28 (12) (1980) 1633–1639.
[34] M.D. Mathew, K. Laha, V. Ganesan, Improving creep strength of 316L stainless steel by alloying with nitrogen, Mater. Sci. Eng., A 535 (2012) 76–83.